LAWRENCE
LIVERMORE
NATIONAL
LABORATORY

UCRL-JRNL-230233

On-chip real-time single-copy polymerase chain reaction in picoliter droplets

N. R. Beer, B. Hindson, E. Wheeler, S. B. Hall, K. A. Rose, I. Kennedy, B. Colston

April 24, 2007

Analytical Chemistry

Updated October 14, 2003

On-chip real-time single-copy polymerase chain reaction in picoliter droplets

*N. Reginald Beer[1,2], Benjamin J. Hindson[1], Elizabeth K. Wheeler[1], Sara B. Hall[1], Klint A. Rose[1], Ian M. Kennedy[2], and Bill W. Colston[1]**

[1]Lawrence Livermore National Laboratory, 7000 East Avenue, Livermore, California 94551, USA

[2]Department of Mechanical and Aeronautical Engineering, University of California, Davis, California 95616, USA

RECEIVED DATE (to be automatically inserted after your manuscript is accepted if required according to the journal that you are submitting your paper to)

*colston1@llnl.gov

ABSTRACT. The first lab-on-chip system for picoliter droplet generation and PCR amplification with real-time fluorescence detection has performed PCR in isolated droplets at volumes 10^6 smaller than commercial real-time PCR systems. The system utilized a shearing T-junction in a silicon device to generate a stream of monodisperse picoliter droplets that were isolated from the microfluidic channel walls and each other by the oil phase carrier. An off-chip valving system stopped the droplets on-chip, allowing them to be thermal cycled through the PCR protocol without droplet motion. With this system a 10-pL droplet, encapsulating less than one copy of viral genomic DNA through Poisson statistics, showed real-time PCR amplification curves with a cycle threshold of ~18, twenty cycles earlier than

commercial instruments. This combination of the established real-time PCR assay with digital microfluidics is ideal for isolating single-copy nucleic acids in a complex environment.

Keywords: on-chip PCR, picoliter PCR, microdroplet, digital microfluidics, real-time PCR, digital PCR, w/o emulsion, qPCR

Introduction

Taqman-based real-time quantitative PCR revolutionized biotechnology by employing a dual-labeled fluorogenic probe to provide accurate quantitation of gene copies[1]. It quickly became the "gold standard" for effectiveness, specificity and sensitivity, and has been used almost exclusively for rapid characterization of pathogens because it does not require post-PCR manipulation and integration with capillary or gel electrophoresis, hybridization arrays, or mass spectrometry[2, 3]. The next advances for rapid detection and characterization focused on reducing the thermal mass and heat diffusion distance into the aqueous sample to decrease PCR cycle time[2]. These advances created a new industry for nucleic acid analysis based on benchtop thermocyclers with integrated optical detection. As these technologies have matured, the cycle time limit has been reached for the μL-scale reactions that these systems perform.

The recent advances in digital microfluidics have dramatically reduced the reaction volumes for performing these types of biochemical reactions. This technology promises high-throughput massively parallel analyses by partitioning the bulk sample into millions of discrete reaction vessels on-chip. In this way each constituent can be isolated and assayed at the single cell[4, 5], virus, protein[6] or nucleic acid level[7-11]. PCR benefits greatly from reactor miniaturization and isolation, especially if the reactors are monodisperse, which ensures consistent reaction rates as well as optical tuning for reactor size. Bulk emulsions are polydisperse, which necessitates higher homogenization speeds to produce smaller droplets with a narrower size distribution[8], but the distribution itself is still Gaussian.

The advantages of digital PCR are well known, principally the ability to detect a single copy of target nucleic acid in a complex background, and it has been used to detect a low concentration of mutations in alleles associated with colorectal cancer[7]. This groundbreaking research demonstrated single molecule sensitivity in a microarray-pipetted sample with a high background. Initially, it required sixty cycles of exponential amplification, followed by ten to fifteen extra cycles of linear amplification for end-point detection using molecular beacon FRET probes.[7] The method has since evolved with commercial arrays, Taqman-based FRET probes, smaller sample volumes, and the forty-cycle PCR protocol; for example, single molecule sensitivity has recently been shown in 6.25nl reaction chambers for multi-gene analysis of individual environmental bacteria.[12] Reducing digital PCR reactor volumes another three orders of magnitude to the picoliter scale would allow earlier detection due to decreased diffusion distances[13], a wider range of sample concentrations, reduced reagent consumption, and improved statistics if all reactors are processed.

Picoliter volume PCR has already been performed in batch-generated emulsions[8-11, 14-16], beads emulsion amplification magnetics (BEAM)[9-11] or microfabricated compartments[17-19], all of which benefit from the reduction of reactor volume. These bulk emulsion PCR methods can only include end-point amplification detection[15]. To perform real-time detection the droplets must be focused into a channel so that background fluorescence from droplets above or below the focal depth does not affect the fluorescence intensity measurement. Otherwise only an average fluorescent intensity measurement is taken, and the optical interrogation of individual reactors, which is key to the digital PCR concept, cannot be performed.

Droplets on a chip, however, offer a level of control over microdroplet compartmentalization not achievable by "shake-and-bake" methods[8-11, 14-16]. Monodisperse droplets with tunable volumes are

generated using microfluidic chips with a T-junction shearing zone and droplet size is adjusted by varying channel geometry, flow rate, and dispersed phase viscosity[20-22].

Combining advanced pL PCR systems such as droplets on-chip with the established Taqman assay allows real-time PCR in isolated picoliter droplets containing single-copy nucleic acids from a complex environmental sample. Here we report on the first on-chip digital microfluidic real-time PCR instrument for generating monodisperse microdroplet reactors, thermal cycling them for PCR, and detecting real-time amplification in the individual picoliter droplets. This method allows detection of a single copy of nucleic acid at significantly reduced cycle thresholds, and will benefit from the high throughput and low reagent usage architecture that on-chip processes provide.

Experimental section

Droplet Generation and chip design To generate water-in-oil (w/o) microdroplets we utilized a chip (Fig. 1a) with hydrophobic channel surfaces and a shearing cross-flow T-junction[20, 22, 23] (Fig 1b). A 0.5 mm-thick silicon wafer was etched in a Deep Reactive Ion Etcher (Surface Technology Systems) and anodic-bonded to a 0.5mm 7740 Pyrex coverslip. Channel surfaces were rendered hydrophobic by flushing with SigmaCote (Sigma-Aldrich) then baking at 100°C for 30 minutes. A steady-state channel flow simulation was developed using the Poiseuille solution to Poisson's equation for steady, incompressible flow in rectangular ducts[24]. Droplet size was estimated from the computed volumetric flow rates, channel hydraulic diameter, carrier fluid viscosity, and surface tension.[23] These analyses indicated that a channel width of 60 μm at the T-junction was optimal for generating 10-picoliter droplets. As seen in Figure 1a, downstream from the droplet generation zone, the channel expands to bring more droplets into the optical field of view, allowing more droplets to be observed while stopped on-chip. Fluid lines connecting to the chip were coupled to eight-port sample injection valves (Valco Instruments, model C22Z-3188EH) for sample loading and synchronized flow stopping. Prior to each run, the fluid lines and channels were

rinsed with a 10% (1.2% m/v, 500 μL) solution of household bleach while the chip was heated to 90 °C, followed by deionized water (1.5 mL).

System Architecture The picoliter droplet real-time PCR instrument is shown schematically in Figure 2. Fluid control was achieved by connecting the chip's three fluid ports to an off-chip valve system. Two infusion syringe pumps (KDScientific) independently drove the aqueous and oil (M8662, Sigma-Aldrich) streams at predetermined flow rates of 2.3 and 0.3mL/hr, respectively. A mixture of nucleic acid sample and PCR reagents were injected into the aqueous stream and delivered to the chip. Stabilizing additives were not required, which greatly simplified translation of the PCR assay to the picoliter regime. The entire chip was thermally cycled using a Melcor 3628 Peltier device with a PID controller (Series 800, Alpha Omega Instruments) programmed for 180 s at 95°C, followed by 40 cycles of 95°C for 20 s, 51°C for 20 s, and 71°C for 10 s and calibrated using thermocouples attached to the silicon surface. The heating and cooling rates were 1.8 °C/s and 1.4 °C/s, respectively. The conservative three-step protocol completed 40 cycles in 108 minutes.

PCR Reagents Per 25 μL, the PCR mastermix contained Accuprime™ Supermix I (Invitrogen), 3 units of Accuprime™ Taq, 0.2 μM forward primer 5′-CAATCTAACTGACGGAGCCCA-3′, 0.2 μM reverse primer 5′-AATGGGTGTTGCCAATGATTC-3′, 0.4 μM 5′FAM-CCCCTGAATATCAATGGATGTCTCCCCATAG-3′BHQ1 probe (Biosearch Technologies), and Vaccinia Western Reserve genomic DNA (Advanced Biotechnologies) 194,711 base pairs (Genbank accession number AY243312.1)[25]. PCR quantification was performed to estimate DNA copy number of our stock template solution. No adjustment for sample loss to the walls of the microfluidics upstream of the chip was made.

Fluorescence detection Fluorescence was monitored using a Nikon TE2000-U microscope fitted with a 41001 FAM Chroma filter set, a 10× Nikon objective and an X-cite Series 120 arc lamp. Fluorescence images were captured with a CoolSnap HQ CCD (1392 x 1040 pixels) with a 100 ms acquisition time. Bright field images were acquired with a MotionPro HS-4 CMOS camera (Redlake) at 5,000 frames per second (512 x 512 pixels). The fluorescence microscope imaged droplets in a 300 x 500 μm section of the channel during the annealing phase of each cycle for real-time detection.

Data Analysis Droplets were identified from bright field images using the Sobel edge detection method[26]. Light-source fluctuations were subtracted from the raw intensity values of all droplets at each cycle. The real-time fluorescence curves were processed using an algorithm adopted from a commercial instrument (SmartCycler Operator Manual D0190 Rev.D, Cepheid, Sunnyvale, CA) to subtract background fluorescence and determine cycle threshold using a threshold value of 0.5 intensity units.

Results and Discussion

With this droplet generation design, the aqueous sample stream encounters the viscous mineral oil cross-flow at the T-junction creating a shear zone. When shear stress overcomes surface tension, the extended aqueous bolus breaks off and quickly relaxes to a spherical geometry as it passes downstream[23]. Figure 1b shows the aqueous bolus at the T-junction with three droplets in succession moving quickly towards the channel center. Downstream, the channel width expands to 300 μm, which decreases droplet separation and increases the droplet density within the field of view. Figure 1c shows an image of monodisperse droplets downstream of the junction, taken prior to stopping the flow. Approximately one-thousand droplets were generated per second. Stopping the flow caused minor flow

perturbations and some coalescence. Once stopped, the droplets remained stationary for the duration of PCR thermal cycling.

Droplets were identified and sized from a bright field image. Monodisperse "singlet" droplets dominated the field, however larger sizes consistent with volume multiples, including doublets, triplets, and higher are visible (see Table 1 for the droplet statistics, including proportion of coalesced to non-coalesced droplets). The observed coalescence occurred during flow stopping, when a small number of droplets in close proximity would collide and fuse. Reducing the channel size to maintain higher droplet spacing would eliminate this phenomenon. We took advantage of this controlled size variation to observe potential droplet size effects. No further coalescence was observed during the entire thermal cycling protocol. The few coalesced droplets with diameters greater than 40 μm were not analyzed. Monodisperse droplet 'singlet' size varied minimally on the same chip device, showing a 2 μm run-to-run variation for the 48 μm etch-depth chip and a 3 μm run-to-run variation for the 64 μm chip. Since the pumps supplied identical volumetric flow rates to both device geometries, the deeper channeled devices had a lower rate of shear at the T-junction, as well as a larger hydraulic diameter, both of which increase generated droplet size.[23]

Our first on-chip PCR results from three separate template concentrations are presented in Figure 3. As discussed, the droplet sizes were measured from the brightfield images (leftmost images in Fig. 3). Fluorescence images were recorded at each thermal cycle. Three characteristic cycles: 1, 16, and 40 are shown for two starting DNA concentrations and the no-template control. The droplet intensities of the complete series of fluorescence images were analyzed to generate the real-time fluorescence curves shown on the far right of Figure 3.

The real-time fluorescence intensity curves for each droplet exhibited exponential, linear, and plateau phases, comparable to microliter-scale reactions performed on commercially available instruments. As can be seen by the droplet intensities, for example in Fig. 3b, the starting fluorescence of a droplet is a

linear function of droplet volume. Very repeatable amplification was observed at 7 starting DNA copies per droplet, whereby all droplets showed successful PCR (Fig. 3a). As expected, the percentage of droplets that supported amplification decreased as the number of starting DNA copies per droplet was reduced (see Table 2 for the observed amplification distribution). A 10-picoliter singlet droplet containing on average ~0.06 copies of DNA and a 20-picoliter doublet droplet containing on average ~0.12 copies supported amplification (Fig. 3b). Poisson statistics (λ=0.05, the distribution's mean) predict 1 out of 21 "singlet" droplets would contain a single copy of DNA. Examining Fig 3b and adjusting the droplet count to include three doublets and two each of the 3x and 4x droplets, gives an equivalent total of 42 droplets, 2 of which showed obvious amplification, in very good agreement with the predicted number from Poisson statistical analysis. Assuming the doublet that amplified started with only one copy of DNA is reasonable, because at this concentration the probability of two droplets containing template, and then coalescing is extremely low. This assumption can not be made for the 0.4 copies per droplet concentration (not shown in Fig. 3), and is most likely why a 6% difference was observed between the experimental percentage of droplets showing amplification and that expected by the Poisson distribution across the equivalent number of singlet droplets (λ=0.4 predicts roughly 1 in 3 droplets will support amplification.) No amplification was observed for the no-template control (Fig. 3c).

The excellent agreement between observed, and Poisson-predicted droplet amplification for the quantitated starting copy concentration across all dilutions shows the promise of picoliter droplets for quantitative PCR (See Table 2). Eliminating coalescence through increased droplet spacing, along with automating the stage to image a greater number of droplets, should provide accurate quantitative PCR, with titer of starting copy determined by the Poisson mean at low concentrations, and cycle threshold at higher concentrations ($\lambda \geq 1$).

The cycle thresholds obtained in picoliter droplets should occur 19.8 cycles earlier than those generated by commercially-available platforms using microliter-scale reactors for the same starting copy number, a result of the 10^6 volume reduction this method employs. We observed this expected Ct shift across all nonzero dilutions (See Table 3). For example, detecting 7 copies in a droplet took only 16.0 cycles, approximately 20 cycles earlier than the same assay conducted in a 25 μL reaction volume. Detecting 0.4 and ~0.06 copies took 17.7 and 18.3 cycles respectively on our device, and over forty cycles when the assay was run on the benchtop instrument. This represents an approximately 56% cycle reduction, and can be coupled with on-chip architectures optimized for rapid heat transfer to vastly reduce analysis time.

We did not observe the 3.3-cycle threshold shift per ten-fold increase in starting copy concentration typical of benchtop PCR. This shift won't be realized unless starting template concentrations greater than 10 copies per droplet are analyzed. This is explained by returning to the Poisson distribution. Once the dilution goes below one copy per droplet, which occurred after our first template concentration, decreasing starting copy should only decrease the number of droplets that support amplification. This is confirmed by the close proximity of cycle thresholds in droplets that amplified on the device (See Table 3). Optimizing the on-chip assay for million-fold smaller reactor volumes, including adjusting polymerase, probe, and primer concentrations should shift the cycle thresholds even lower by improving the amplification efficiency.

Future directions of this research will focus on optimizing the assay for the picoliter scale emulsion, redesigning the device channels to increase droplet spacing, interrogating the entire device, and demonstrating this method on different bacterial and viral genomes.

Conclusions

We have demonstrated a six order of magnitude reactor size reduction from commercial real-time PCR systems, using a method of sample partitioning into monodisperse picoliter droplets emulsified in oil on-chip, where the reactors can be further manipulated and interrogated individually in real time. The described method required only eighteen cycles for single-copy real-time detection on-chip using Taqman-based FRET probes. The isolated droplets are a million-fold smaller than array-based PCR, enabling a significant reduction in required cycles to detection, and subsequent transport, manipulation, and archival of the droplets. The method is well-suited to qPCR applications, given the observability of Poisson statistics in a picodroplet-discretized sample. Adaptation of rapid microfluidic thermal cycling strategies[27], coupled with reduced cycles will further increase throughput. Applying digital microfluidics to real-time PCR combines the advantages of on-chip processing of picoliter reactors with the detection of single-copy target nucleic acids from a complex environment.

References

(1) Heid, C. A.; Stevens, J.; Livak, K. J.; Williams, P. M. *Gen. Res.* **1996**, *6*, 986-994.
(2) Belgrader, P.; Benett, W.; Hadley, D.; Richards, J.; Stratton, P.; Mariella, R.; Milanovich, F. *Science* **1999**, *284*, 449-450.
(3) Belgrader, P.; Elkin, C. J.; Brown, S. B.; Nasarabadi, S. N.; Langlois, R. G.; Milanovich, F. P.; Colston, B. W.; Marshall, G. D. *Anal. Chem.* **2003**, *75*, 3446-3450.
(4) He, M. Y.; Edgar, J. S.; Jeffries, G. D. M.; Lorenz, R. M.; Shelby, J. P.; Chiu, D. T. *Anal. Chem.* **2005**, *77*, 1539-1544.
(5) Tan, Y. C.; Hettiarachchi, K.; Siu, M.; Pan, Y. P. *J. Am. Chem. Soc.* **2006**, *128*, 5656-5658.
(6) Wheeler, A. R.; Moon, H.; Bird, C. A.; Loo, R. R. O.; Kim, C. J.; Loo, J. A.; Garrell, R. L. *Anal. Chem.* **2005**, *77*, 534-540.
(7) Vogelstein, B.; Kinzler, K. W. *Proc. Natl. Acad. Sci.* **1999**, *96*, 9236-9241.
(8) Miller, O. J.; Bernath, K.; Agresti, J. J.; Amitai, G.; Kelly, B. T.; Mastrobattista, E.; Taly, V.; Magdassi, S.; Tawfik, D. S.; Griffiths, A. D. *Nat. Meth.* **2006**, *3*, 561-570.
(9) Diehl, F.; Li, M.; He, Y. P.; Kinzler, K. W.; Vogelstein, B.; Dressman, D. *Nat. Meth.* **2006**, *3*, 551-559.
(10) Williams, R.; Peisajovich, S. G.; Miller, O. J.; Magdassi, S.; Tawfik, D. S.; Griffiths, A. D. *Nat. Meth.* **2006**, *3*, 545-550.
(11) Dressman, D.; Yan, H.; Traverso, G.; Kinzler, K. W.; Vogelstein, B. *Proc. Natl. Acad. Sci.* **2003**, *100*, 8817-8822.
(12) Ottesen, E. A.; Hong, J. W.; Quake, S. R.; Leadbetter, J. R. *Science* **2006**, *314*, 1464-1467.

(13) Jensen, K. *Nature* **1998**, *393*, 735-+.
(14) Nakano, M.; Komatsu, J.; Matsuura, S.; Takashima, K.; Katsura, S.; Mizuno, A. *J. Biotechnol.* **2003**, *102*, 117-124.
(15) Musyanovych, A.; Mailander, V.; Landfester, K. *Biomacromolecules* **2005**, *6*, 1824-1828.
(16) Nakano, M.; Nakai, N.; Kurita, H.; Komatsu, J.; Takashima, K.; Katsura, S.; Mizuno, A. *J. Biosci. Bioeng.* **2005**, *99*, 293-295.
(17) Nagai, H.; Murakami, Y.; Morita, Y.; Yokoyama, K.; Tamiya, E. *Anal. Chem.* **2001**, *73*, 1043-1047.
(18) Marcus, J. S.; Anderson, W. F.; Quake, S. R. *Anal. Chem.* **2006**, *78*, 956-958.
(19) Leamon, J. H.; Lee, W. L.; Tartaro, K. R.; Lanza, J. R.; Sarkis, G. J.; deWinter, A. D.; Berka, J.; Lohman, K. L. *Electrophoresis* **2003**, *24*, 3769-3777.
(20) Thorsen, T.; Roberts, R. W.; Arnold, F. H.; Quake, S. R. *Phys. Rev. Lett.* **2001**, *86*, 4163-4166.
(21) Tan, Y. C.; Fisher, J. S.; Lee, A. I.; Cristini, V.; Lee, A. P. *Lab Chip* **2004**, *4*, 292-298.
(22) Garstecki, P.; Fuerstman, M. J.; Stone, H. A.; Whitesides, G. M. *Lab Chip* **2006**, *6*, 437-446.
(23) Cristini, V.; Tan, Y. C. *Lab Chip* **2004**, *4*, 257-264.
(24) White, F. M. *Viscous Fluid Flow,* 3rd ed.; McGraw-Hill, 2006.
(25) Benson, D. A.; Karsch-Mizrachi, I.; Lipman, D. J.; Ostell, J.; Rapp, B. A.; Wheeler, D. L. *Nucleic Acids Res.* **2000**, *28*, 15-18.
(26) Gonzalez, R. C., Woods, R.E. *Digital Image Processing*, 2nd ed.; Prentice Hall, 2002.
(27) Kopp, M. U.; de Mello, A. J.; Manz, A. *Science* **1998**, *280*, 1046-1048.

Acknowledgements. We thank Chance Carter, Bill Benett, Julie Hamilton, and Lance Bentley Tammero for technical assistance. This work was performed under the auspices of the U. S. Department of Energy by the University of California, Lawrence Livermore National Laboratory (LLNL) under Contract No. W-7405-Eng-48. The project #06-ERD-064 was funded by the Laboratory Directed Research and Development Program at LLNL.

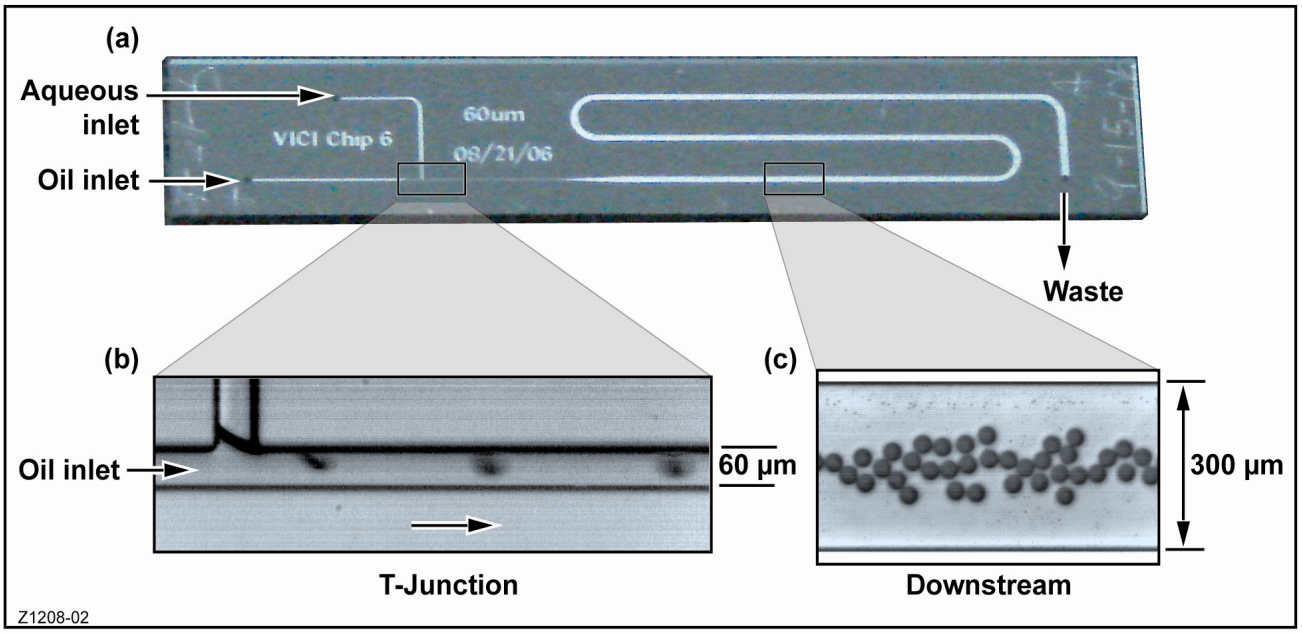

Figure 1. Images of the PCR chip showing **a**, the overall channel and flow configuration, **b**, droplet generation at the T-junction and **c**, monodisperse droplets in the downstream channel.

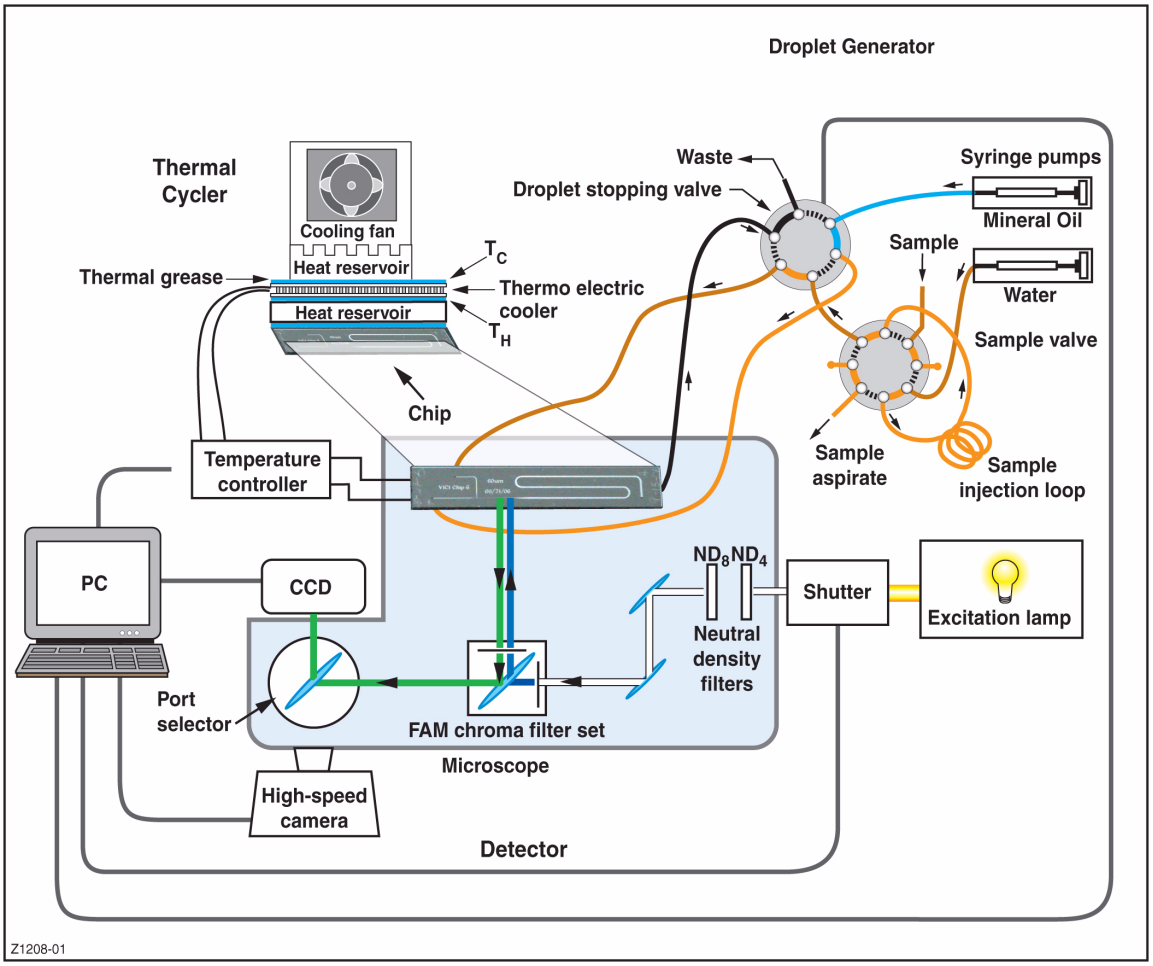

Figure 2. Schematic of the instrument for real-time PCR in picoliter droplets showing the integrated droplet generator, thermal cycler and fluorescence detector.

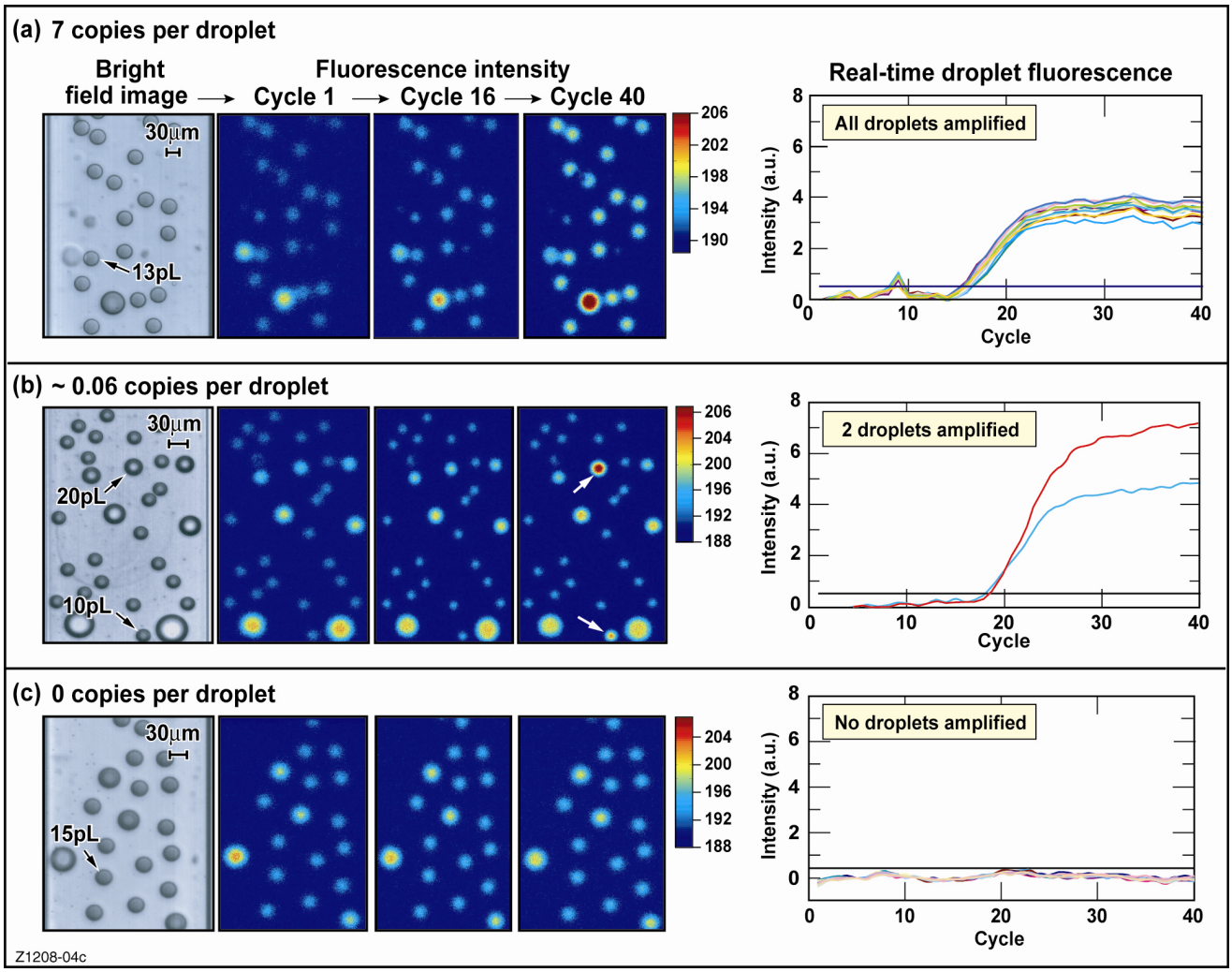

Figure 3. Real-time PCR data from picoliter droplets at an estimated **a**, 7 **b**, ~0.06 and **c**, zero copies of genomic DNA per singlet droplet. Droplets were identified from the bright field image, then monitored at each cycle to generate real-time fluorescence curves. In **a**, all droplets amplified, whereas in **b** only 2 droplets amplified (white arrows). No amplification was observed from **c** the negative control.

Table 1. Droplet statistical analysis across four dilutions

Copies of genomic DNA per singlet droplet		7	0.4	~0.06	0
Droplet Number	Total # in brightfield image	19	29	29	17
	# of singlet droplets	18	18	22	14
	# of doublet droplets	0	6	3	2
Singlet droplet Size	Average diameter (μm)	29*	24‡	27‡	31*
	Diameter standard deviation (μm)	0.4	1.2	0.1	0.3
	Average volume (pL)	13	8	10	15

*Droplets formed in 64μm deep channel; ‡droplets formed in 48μm deep channel. The observed larger droplet size for the 64μm chip device is due to reduced shear rate at the T-junction & increased channel hydraulic diameter[23].

Table 2. Comparison of observed amplification distribution to Poisson statistics

Copies of genomic DNA per singlet droplet	7	.4	~0.06	0
% of droplets with successful amplification	100	27[+]	5[+]	0
Poisson predicted % of droplets with successful amplification	100	33[Δ]	6	0

[+] For the percentage calculation the total number of droplets was adjusted by counting coalesced droplets as their equivalent number of singlet droplets. [Δ] Difference between the observed and Poisson predicted value is attributed to some coalesced droplets containing more than one starting template copy at this concentration

Table 3. Comparison of picoliter droplet cycle thresholds to a commercial real-time instrument

Copies of genomic DNA per singlet droplet	7	.4	~0.06	0
Cycle threshold (Ct)	15.98	17.73	18.25	N/A
Ct standard deviation	0.396	1.258	N/A	N/A
Ct on benchtop instrument with same copy number	36.36	40.44*	40.44*	N/A
ΔCt	20.38	22.71	22.19	N/A

* Represents the single-copy limit of our assay on the commercial instrument.